Design and performance optimization of the pneumatic precision peanut planter with combined positive-negative pressure

Yan Yu[1,2,3], Weikang Dong[1,2,3], Cheng Yang[1,2,3*], Yushuai Song[1,2,3], Jun Liu[1,2,3], Yushuai Li[1,2,3]

(1. *College of Mechanical and Electrical Engineering, Qingdao Agricultural University, Qingdao 266109, Shandong, China*;
2. *Qingdao Plantech Mechanical Technology Co, Ltd, Qingdao 266109, Shandong, China*;
3. *Collaborative Innovation Center for Shandong's Main Crop Production Equipment and Mechanization, Qingdao 266109, Shandong, China*)

Abstract: To address the issue of insufficient accuracy and stability in pneumatic peanut planters during high-speed operations (above 8 km/h), this study designs a peanut precision planter based on combined positive and negative pressure, and improves its performance via multi-dimensional optimization. The research uses Shandong "Silihong" peanuts as the study subject, determining their geometric characteristics and designing the core parameters of the seed-metering disc: diameter of 255 mm, 21 suction holes, and suction hole diameter of 6.2 mm. A comparative simulation using EDEM discrete element method between the arc-shaped and spoke-wing groove seed disturbance structures shows that the spoke-wing groove structure increases the average seed speed by 17.0%, significantly improving the seed filling effect. A coupled Fluent-EDEM gas-solid simulation confirmed the optimal negative pressure to be 6.0 kPa, achieving a single-seed adsorption rate of 98.6%. Orthogonal experiments were performed to optimize the operating parameters, and the optimal combination with corresponding sowing performance indices was obtained. Field tests indicated that the performance of the planter meets the national standards for precision sowing when the operating speed is ≤12 km/h.

Keywords: pneumatic seed-metering device, peanut precision seeding, structural optimization of seed-metering disc, discrete element simulation (EDEM), gas-solid coupling simulation, performance optimization
DOI: 10.25165/j.ijabe.20261903.10129

Citation: Yu Y, Dong W K, Yang C, Song Y S, Liu J, Li Y S. Design and performance optimization of the pneumatic precision peanut planter with combined positive-negative pressure. Int J Agric & Biol Eng, 2026; 19(3): 89–98.

1 Introduction

Peanut, as an important global oilseed and economic crop, is rich in fats and proteins, playing a strategic role in ensuring food and oil security[1-3]. In China, the peanut planting area exceeds 70 million acres, and the total production has ranked first globally for 20 consecutive years, accounting for more than 35% of the world's total production[4,5]. As a key link in peanut production, sowing directly affects the improvement of yield and industrial efficiency. Thus, technological breakthroughs are necessary through equipment innovation to overcome technical bottlenecks[6-9].

Traditional precision sowing faces numerous challenges, including the fragility of peanut seeds, which are prone to damage. The poor adhesion of the seed coat (or "red skin") often leads to peeling. Existing mechanical devices fail to meet the agronomic requirements[10]. The performance of current pneumatic seed planters is constrained by factors such as positive and negative pressures and rotational speed. Pressure imbalances lead to missed or double sowing, while improper rotation speed reduces performance. Optimizing the matching of these factors is critical to enhancing performance[11].

As the core executing component in precision sowing, the performance of seed-metering devices directly influences sowing uniformity and seed utilization[12]. Based on operational mechanisms, mainstream seed-metering devices can be categorized into mechanical and pneumatic types[13]. Among these, pneumatic seed-metering devices have become a key research direction for large-scale planting equipment due to their high-speed adaptability and low damage characteristics.

The development of international pneumatic seed dispensing technology began in the 1950s, with Russian scholars first proposing the pneumatic seed pickup theory, followed by accelerated industrialization in Europe and the United States. The composite seed-metering disc developed by the French company Monosem[14] balances durability and mechanical performance. The Manemerge planters series developed by the American company John Deere[15] achieves multi-grain compatibility sowing for crops like soybeans and corn, with a qualified seed-spacing rate of 97%. In terms of basic theoretical research, He et al.[16] constructed a combined suction hole dynamics model and revealed the nonlinear effects of vacuum degree (–3 to –5 kPa) and suction hole linear velocity (0.2-0.5 m/s) on single-seed adsorption probability. Chen's team[17] used ANSYS vortex field simulation to confirm that conical suction holes reduce airflow disturbance by 28%.

Current research trends focus on improving adaptability across multiple operational conditions: Yi et al.[18] developed a composite positive-negative pressure hole-wheel structure, controlling the grain sowing overlap rate to ≤3% through air pressure gradient

Received date: 2025-08-23 **Accepted date:** 2026-04-17
Biographies: Yan Yu, PhD, Professor, research interest: intelligent agricultural equipment, Email: 18354673839@163.com; **Weikang Dong**, MS candidate, research interest: agricultural engineering and information technology, Email: 2628342926@qq.com; **Yushuai Song**, MS candidate, research interest: agricultural machinery equipment engineering, Email: 1006213566@qq.com; **Jun Liu**, MS candidate, research interest: agricultural machinery equipment engineering, Email: liuuu5980@163.com; **Yushuai Li**, MS candidate, research interest: agricultural electrification and automation, Email: liyushuaili@163.com.
***Corresponding author: Cheng Yang**, MS, Senior Engineer, research interest: intelligent agricultural equipment. R&D Department, Qingdao Plantech Mechanical Technology Co, Ltd, Qingdao 266109, China. Tel: +86-15689101168, Email: ycplantech@126.com.

control. The Tang Han team[19] designed a high-speed corn planter using flexible sealing technology, enabling sowing speeds exceeding 15 km/h, thus providing a new approach for pneumatic seed adsorption and air-assisted seed delivery for fragile seeds like peanuts. Despite these advances, there remains a gap in research aimed at addressing the unique physical and biological properties of peanut seeds, with high-efficiency adaptable seed-metering devices still lacking, which requires further exploration and refinement[20-22].

Therefore, this study developed a pneumatic peanut precision seed-metering device based on combined positive and negative pressure. The geometric characteristics of peanut seeds were first measured to determine the key structural parameters of the seed-metering disc. Then, the spoke-wing groove disturbing structure was optimized by DEM simulation, and the optimal negative-pressure level was verified by Fluent-EDEM coupled simulation. Finally, orthogonal bench experiments and field tests were conducted to evaluate the working performance of the developed device. The results provide a theoretical and experimental basis for improving peanut precision sowing under high-speed operating conditions.

2 Overall structure and working principle

2.1 Overall structure

The pneumatic peanut precision seed-metering device mainly includes a seed box, a seed-box end shell, a seed-cleaning plate, a seed-metering disc, a negative-pressure end shell, and a seed-guiding device, as shown in Figure 1. Among them, the seed-metering disc is the core component for seed pickup and transport, while the other components cooperate to ensure stable seed cleaning and seed delivery. The working principle of the device is described in Section 2.2.

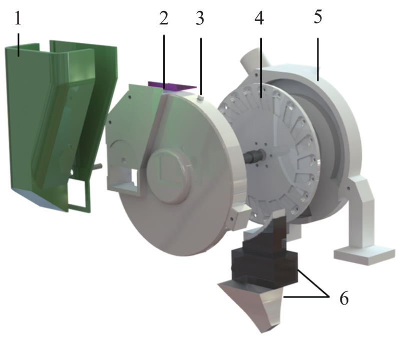

1. Seed box 2. End shell of the seed box 3. Seed cleaning plate 4.Seed-metering disc 5. Negative pressure end shell 6. Seed guidance device

Figure 1 Schematic diagram of the pneumatic peanut seed distributor structure

2.2 Working principle

The working process of the pneumatic peanut precision seed-metering device includes seed pickup under negative pressure, seed cleaning for single-seed selection, seed release in the unloading zone, and seed delivery through the positive-pressure seed-guiding system, as shown in Figure 2. The fan system provides a stable negative-pressure field to the seed-metering disc through the airflow channel. Under the action of negative pressure, peanut seeds in the seed chamber are attracted to the suction holes on the rotating seed-metering disc and move synchronously with the disc. When the seeds enter the seed-cleaning zone, excess seeds attached to the suction holes are removed by the cleaning device to ensure single-seed pickup. As the adsorbed seeds rotate to the unloading zone, they are released under the combined action of gravity and the unloading mechanism, and then enter the seed-guiding tube. Finally, the seeds are transported accurately into the seed trench through the positive-pressure seed-guiding system.

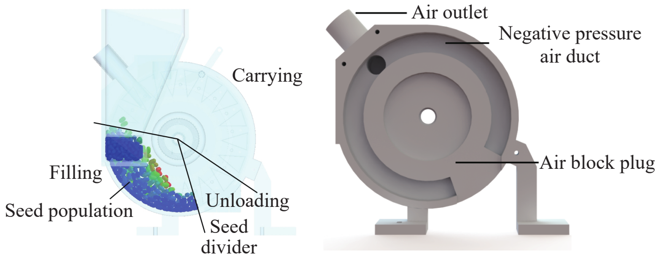

Figure 2 Workflow diagram of air-driven peanut seed distributor

Under high-speed operating conditions, the combined positive-negative pressure design improves both seed pickup stability and seed discharge continuity. Negative pressure helps maintain reliable seed adsorption during disc rotation, thereby reducing missed seeding caused by insufficient suction. At the same time, positive pressure in the seed-guiding system accelerates seed conveying and reduces seed retention or blockage in the guiding channel, which is beneficial to stable seed delivery and uniform seed spacing during high-speed sowing.

3 Seed-metering disc design

3.1 Geometric characteristics of peanut seeds

The seed-metering disc is a key component in the seed-metering device, driving seeds through various zones to achieve single-seed sowing during the operation. The design parameters of the seed-metering disc are primarily based on the geometric characteristics of the seeds[23]. This study selects the four-grain red peanut seeds, commonly used in Shandong Province, as the experimental subject. A total of 100 peanut seeds were randomly selected, and their length, width, and height were measured using a Vernier caliper. The dimensions of the three axes are listed in Table 1.

Table 1 Three-axis dimensional parameters

Parameter	Length/mm	Width/mm	Thickness/mm
Max value	18.30	10.40	9.30
Min value	10.10	6.60	6.30
Average value	14.30	7.80	7.40
Standard deviation	1.37	0.63	0.55

From the measurement data, it can be observed that the average three-axis dimensions of the four-grain red peanut seeds are 14.3 mm×7.8 mm×7.4 mm.

3.2 Seed-metering disc design

The design parameters of the seed-metering disc will directly affect the stability of the seed pickup, cleaning, transportation, and sowing stages[24,25]. An equation system is established to analyze the impact of these parameters on its seed-filling performance[26].

$$\begin{cases} t = \dfrac{l_h}{v_p} \\ l_h = \delta_c \dfrac{D - \Delta d}{2} \\ V_p = \pi n_p \dfrac{D - \Delta d}{60} \end{cases} \tag{1}$$

where, t is dwell time of the seed-metering disc in the seed-filling area, s; l_h is arc length of the seed-filling area, mm; V_P is linear speed of the seed-metering disc, m/s; δ_c is radian of the seed-filling area, rad; D is diameter of the seed-metering disc, mm; n_p is rotational speed of the seed-metering disc, r/min; Δd is difference between the diameter of the seed-metering disc and the circumferential diameter of the seed-suction hole, mm.

From the above equation, it can be concluded that the residence time of the seed-metering disc in the seed-filling area is solely related to the angle of the area and the rotational speed of the seed-metering disc.

Based on the design, the turning angle θx of the seed-filling area is 120°, and the arc length of the seed-filling area is approximately $\pi D/3$. Substituting this into Equation (2) and simplifying gives:

$$t = \frac{2\pi}{3\omega} \tag{2}$$

where, the seed-filling time tx is inversely proportional to the rotational angular velocity ω of the seed-metering disc, and thus inversely proportional to the rotational speed n of the seed-metering disc. Based on the structure of the seed-metering device's air chamber and related literature, the diameter D of the seed-metering disc is determined to be 255 mm. The material selected for construction is photosensitive resin with a thickness of 8 mm.

3.3 Design of suction hole number on the seed-metering disc

The number of seed pickup holes on the seed-metering disc can be calculated using Equation (3)[27].

$$n_1 = \frac{V_t \pi d_1 (1 - S_r)}{3.6Av} \tag{3}$$

where, n_1 is number of suction holes; V_t is travel speed of the tractor, km/h; d_1 is diameter of the seed-metering disc, mm; S_r is slip ratio of the tractor, %; A is peanut plant spacing, mm; v is linear speed of the seed-metering disc, m/s.

The average speed of the tractor is taken as 8 km/h, the diameter of the seed-metering disc is 255 mm, and based on a plant spacing of 155 mm[28,29] and a rotational speed of 40 r/min, the number of seed pickup holes is calculated to be 21 by substituting the values into Equation (3).

3.4 Seed pickup hole diameter parameter design

The design parameters of the seed pickup holes play a decisive role in the seed pickup performance of the seed-metering device. To determine the diameter of the seed pickup holes, the three-axis dimensions of the measured peanut seeds are required. In this study, the average three-axis dimensions of four red peanut seeds are used for the sample selection calculation.

The equivalent diameter of the peanut seeds[30] is calculated using the following equation:

$$D = \sqrt[3]{L \times W \times T} \tag{4}$$

where, D is equivalent diameter of peanut, mm; L is average length of peanut, mm; W is average width of peanut, mm; T is average thickness of peanut, mm.

The empirical equation for determining the diameter of seed pickup holes on the seed-metering disc, as referenced from the *Agricultural Machinery Design Manual*, is given by:

$$d_3 = (0.64 \sim 0.66) \times D \tag{5}$$

By substituting the measured three-axis dimensions of the seeds into Equations (4) and (5), the equivalent diameter of the "Four Red" peanut variety is calculated to be 9.44 mm. The corresponding diameter of the seed pickup hole on the seed-metering disc ranges between 6 mm and 6.3 mm. For the force analysis and simulation analysis, the diameter of 6.2 mm is initially used for calculations.

4 Simulation experiment and structural design optimization

4.1 Optimization design of the peanut seed-metering disc disturbance structure

The issues of low seed-filling efficiency in traditional seed-metering devices were addressed based on discrete element method (DEM) simulation. Two novel disturbance structure seed-metering discs were designed: an arc-type structure and a spoke-slot structure, as shown in Figure 3. The geometric parameters and arrangement of the disturbance plates are optimized to enhance the fluidization and distribution of seeds [31-34]. A control group without disturbance is set up, and three parallel experiments are conducted using EDEM simulation to explore the mechanisms through which different structures improve seed-filling performance. Based on the discrete element contact mechanics model, the movement trajectory and forces acting on the seed group within the disturbance slots are analyzed to identify the optimal structure.

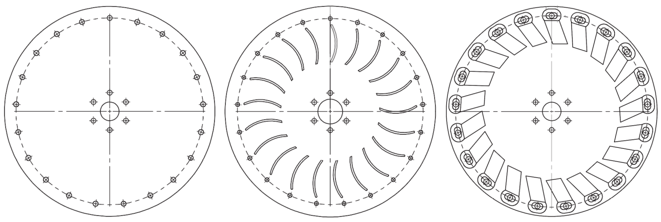

Figure 3 Different specifications of seed-metering discs

4.2 Model establishment

This study analyzed the disturbance characteristics of the seed population in the filling chamber formed by the seed box and seed-metering disc. A simplified model of the seed-metering system is shown in Figure 4. Using "Silihong" peanut seeds as the research object[35], a multi-sphere particle model was established in EDEM based on the measured geometric parameters, as shown in Figure 5.

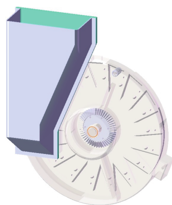

Figure 4 Simplified seed dispensing mechanism model

Figure 5 Peanut seed model

Using the discrete element simulation software EDEM, the disturbance effects of different seed-metering discs on peanuts are investigated. Three sets of seed-metering disc simulation experiments are conducted with a rotational speed of 40 r/min and 500 peanuts, measuring the average velocity of the seed group as the performance indicator[36]. Based on the measurement of the three-axis dimensions of the "Four Red" peanut seeds, as shown in Figure 5, and assuming a normal distribution with a standard deviation of 0.05, the Hertz-Mindlin no-slip contact model is selected, with contact parameters as listed in Table 2.

Table 2 Simulation parameters for mechanical properties

Items	Parameters	Values
Seed Particle	Poisson's ratio	0.36
	Shear modulus/Pa	1.86×10^7
	Density/kg·m^{-3}	1050
ABS Material	Poisson's ratio	0.39
	Shear modulus/Pa	8.9×10^8
	Density/kg·m^{-3}	1100
Nylon Material	Poisson's ratio	0.40
	Shear modulus/Pa	1.1×10^9
	Density/kg·m^{-3}	1140
Peanut-Peanut	Restitution coefficient	0.50
	Static friction coefficient	0.21
	Kinetic friction coefficient	0.04
Particle-ABS	Restitution coefficient	0.51
	Static friction coefficient	0.30
	Kinetic friction coefficient	0.01
Particle-Nylon	Restitution coefficient	0.60
	Static friction coefficient	0.30
	Kinetic friction coefficient	0.30

4.3 Discrete element simulation results and analysis

During the DEM simulation, the seed-metering disc rotated at a constant speed, and the movement of the peanut seed population in the filling chamber was monitored in real time. As shown in Figure 6, a monitoring region was defined to extract the average seed-population velocity over one rotation cycle, which was used to evaluate the fluidization state of the seed population and the disturbance performance of different disc structures.

Figure 7 compares the variation in average seed-population velocity for the non-disturbing seed-metering disc, the arc-disturbing structure, and the spoke-wing groove disturbing structure. The results show that, under the same rotational speed, the spoke-wing groove disturbing structure produced a more stable and effective disturbance effect on the peanut seed population than the other two structures. Compared with the non-disturbing structure, the spoke-wing groove structure improved seed-population fluidization and promoted more uniform seed movement in the filling chamber. Therefore, the spoke-wing groove disturbing structure was selected for further parameter analysis.

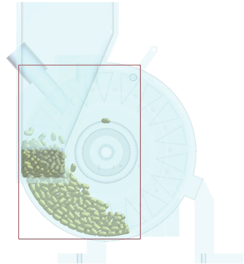

Figure 6 Detection region in the seed-filling chamber

To further determine the structural parameters of the disturbing groove, discrete element simulations were conducted by varying groove depth and groove length. The groove depth was set to 2, 3, and 4 mm, and the groove length was set to 20, 30, and 40 mm. The average seed-population velocity was used as the evaluation index to analyze the influence of these parameters on the fluidization performance of the seed population.

As shown in Figure 8, under the baseline structural parameters of groove length 30 mm and groove depth 2 mm, the average seed-population velocity was 0.1373 m/s. Increasing groove depth significantly enhanced the disturbance effect and improved seed-population fluidization. When the groove depth increased from 2 to 4 mm at a fixed groove length of 30 mm, the average seed-population velocity increased significantly. Compared with groove length, groove depth showed a stronger influence on seed motion. This indicates that groove depth is the dominant structural factor affecting the disturbance performance of the seed-metering disc.

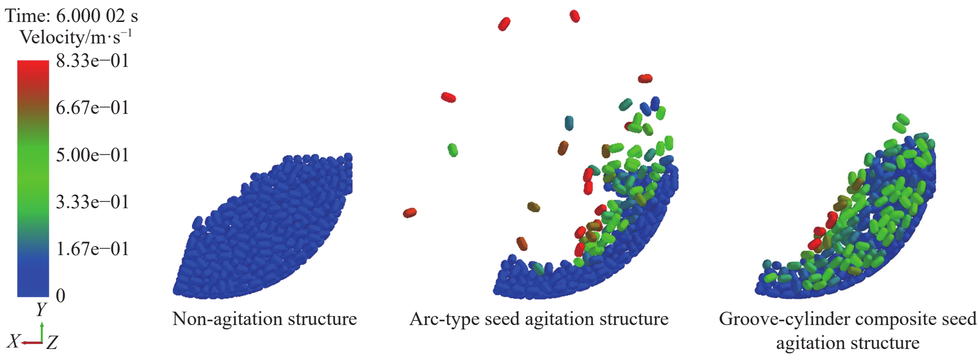

Figure 7 Comparison chart of disturbance effects

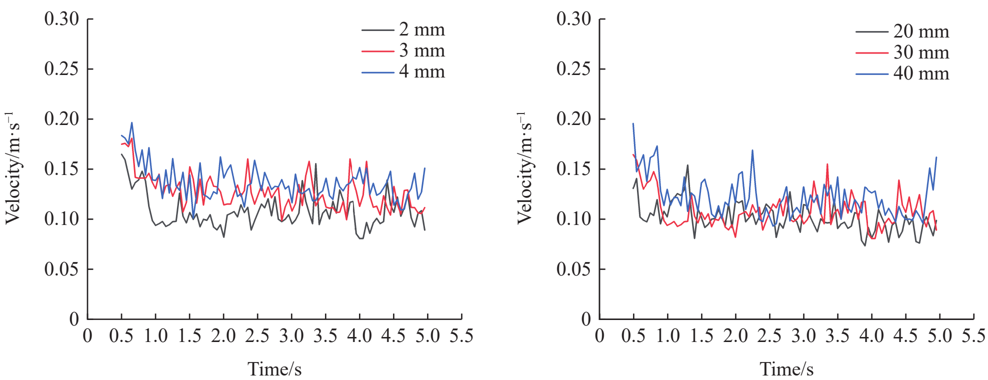

Figure 8 Comparison of seed population velocities

Considering both the improvement in seed-filling performance and the manufacturability of the seed-metering disc, a groove depth of 4 mm and a groove length of 40 mm were selected as the structural parameters of the spoke-wing groove disturbing structure. Under this optimized parameter combination, the average seed-population velocity increased to 0.1706 m/s, indicating that the optimized disturbing structure can effectively improve seed-population fluidization and create more favorable conditions for stable seed filling.

4.4 Fluent-EDEM-based gas-solid coupling simulation validation

To further verify the influence of seed-disturbing structure parameters on gas-solid two-phase flow, supplementary Fluent-EDEM coupled simulations were conducted to quantify the synergistic effect between the airflow field and seed movement. The simulation parameters are set as follows:

Geometric model: The simplified model of the seed-metering device from EDEM was adopted, including a seed-disturbing structure with a groove depth of 4 mm and length of 40 mm, a seed-metering disc with a diameter of 255 mm, and 21 suction holes.

Fluid parameters: The medium is air, with a negative pressure parameter of 5-7 kPa; the wall was set with a no-slip condition.

Coupling settings: Bidirectional data transfer was achieved through an interface. Fluent calculated the drag force and pressure gradient force of the airflow on particles, while EDEM fed back particle positions and velocities to the flow field calculation. The simulation duration was 6 s with a time step of 0.001 s.

Significant differences in seed adsorption and airflow field distribution were observed under the three groups of negative pressures, as shown in Figure 9.

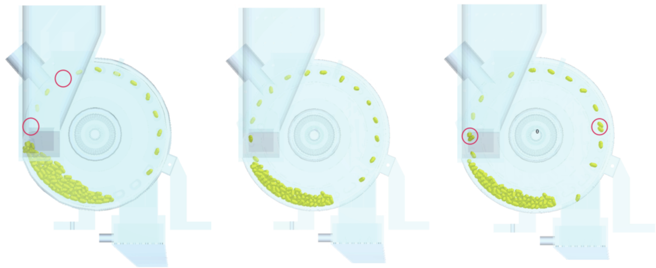

a. 5 KPa b. 6 KPa c. 7 KPa

Figure 9 Comparative experimental diagram of coupling simulation

At 5 kPa negative pressure: Approximately 15.3% of the suction holes exhibited miss-adsorption (Figure 9a), verifying that insufficient negative pressure inhibits seed-filling performance.

At 6 kPa negative pressure: The pressure gradient was balanced by the seed gravity and friction force, resulting in a single-seed adsorption rate of 98.6% (Figure 9b) without miss-adsorption or multi-adsorption, indicating the optimal gas-solid synergistic effect.

At 7 kPa negative pressure: Excessive negative pressure led to the formation of strong eddy currents near the suction holes, with 12.7% of the holes showing multi-adsorption of 2 seeds (Figure 9c). The seed collision frequency increased by 23.1%, and the risk of seed coat damage rose.

The coupling simulation results demonstrate that 6 kPa negative pressure achieves the best balance between adsorption capacity and airflow stability, effectively preventing insufficient seed adsorption at 5 kPa and multi-seed adsorption at 7 kPa.This provides a direct basis for air pressure parameter matching at the gas-solid coupling level.

4.5 Seed dispensing process analysis

In the pneumatic peanut seed-dispensing device, the peanut seeds enter the seed guide channel under the influence of gravity and the pneumatic field. Figure 10A shows the dynamic force analysis of individual seeds detaching from the seed-metering device and entering the inlet section of the seed guide tube. The initial seed velocity is determined by the circumferential velocity of the seed-metering disc and the pneumatic propulsion, based on which a two-dimensional kinematic equation is established:

$$\begin{cases} v_x(t) = v_p \cdot \sin\alpha + \dfrac{F_{\text{net,x}}}{m} \cdot t \\ v_y(t) = v_p \cdot \cos\alpha + \dfrac{F_{\text{net,y}}}{m} \cdot t \end{cases} \tag{6}$$

where, v_p is the absolute initial velocity of the peanut seed entering the seed-guiding tube, m/s; m is the mass of the peanut seed, kg; and t is the motion time, s.

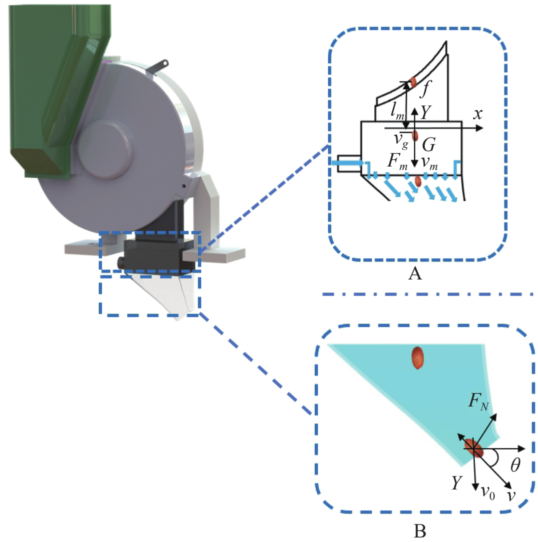

Figure 10 Diagram of the seed introduction process of peanuts

Considering that the seed's posture has little effect on acceleration during the accelerating fall, the model simplifies the peanut seed as a sphere. In the stable acceleration zone, the seed is subjected to both the airflow thrust and gravity in the vertical direction. After a time t, the displacement accelerated by the airflow is l_m. Based on Newton's second law, the acceleration equation is derived.

$$F_m + G - f = \frac{\rho_m \pi d^3}{6} \times 10^{-9} \cdot \frac{d^2 v_m}{dt^2} \tag{7}$$

where, ρ_m represents the density of the peanut seeds, with units of kg/m^3; dm is the equivalent diameter of the peanut seeds, with units of mm; v_m is the instantaneous velocity of the seeds in the acceleration zone, with units of m/s. The calculation expression for the airflow thrust F_m is as follows:

$$F_m = \frac{C_d \pi \rho_g}{8} \times \left(v_g - v_m\right)^2 \cdot d_m^2 \tag{8}$$

where, ρ_g is the air density, kg/m^3; v_g is the average airflow velocity in the acceleration zone, m/s; C_d is the drag coefficient of the peanut seed[35]. Since the main forces acting on the seed during acceleration are the airflow drag force F_d and gravity G, the motion characteristics are derived by solving the system of differential equations formed by Equations (7) and (8).

$$\frac{dv_m}{dt} = \frac{3C\rho_g}{4\rho_m d_m}(v_g - v_m)^2 + \frac{G}{\pi d_m^3 \rho_m / 6\times 10^9} \tag{9}$$

$$\frac{dl_m}{dv_m} = \frac{v_m}{\frac{dv_m}{dt}} = \frac{4\rho_m d_m v_m}{3C\rho_g(v_g - v_m)^2} + \frac{\pi d_m^3 \rho_m v_m}{6\times 10^9 G} \tag{10}$$

where, l_m is the downward displacement of the peanut seed in the acceleration zone, mm. The differential Equations (9) and (10) characterize the kinematic behavior of the seed in the acceleration zone of the pneumatic seed-metering device. The theory shows that the acceleration vector of the seed is significantly positively correlated with the effective velocity gradient of the positive pressure airflow in the stable acceleration zone. Optimizing the seed guide tube structure parameters to improve internal pressure is one of the core strategies for efficient and precise peanut seeding.

To further analyze the complex motion of the peanut seed inside the seed guide tube, a rectangular coordinate system is established with the seed's center of mass as the origin (the horizontal direction is the x-axis, and the vertical downward direction is the y-axis), as shown in Figure 10B. In this coordinate system, the resultant force in the x-axis direction can be expressed as following equation:

$$\sum F_x = (F_m - f)\cos\theta \tag{11}$$

where, γ represents the instantaneous direction of the peanut seed's motion relative to the vertical direction (y-axis), i.e., the seed's tilt angle; f is the sliding frictional force between the seed and the inner wall of the seed guide tube, $f = \mu N$ (μ is the coefficient of friction, and N is the normal force at the contact surface). The thrust F_m exerted on the seed in the airflow field is closely related to the airflow parameters:

$$\begin{cases} F_m = \frac{1}{2}AC\rho_g u^2 \\ u^2 = \frac{2P}{\rho_g} \end{cases} \tag{12}$$

where, P represents the local static pressure of the airflow inside the seed guide tube, Pa; A is the projected area of the seed in the direction of airflow (the windward area), m^2; u is the airflow velocity near the position of the seed, m/s.

In the seed release area (typically near the seed guide tube outlet), the final release velocity of the peanut seed is expressed as:

$$v = v_0 + \frac{\sum F_x}{m}t \tag{13}$$

where, v_0 represents the initial velocity of the peanut seed entering the release zone, m/s; v is the final release velocity of the seed, m/s. By combining Equations (11)-(13), the seed release velocity can be simplified as follows:

$$\begin{aligned} v &= v_0 + \frac{\left(\frac{1}{2}AC\rho_g \cdot \frac{2P}{\rho_g} - f\right)\cos\theta}{m}t \\ v &= v_0 + \frac{(APC - f)\cos\theta}{m}t \end{aligned} \tag{14}$$

Further analysis of Equation (14) shows that the release velocity of the peanut seeds is influenced by the angular velocity of the seed-metering disc, the pneumatic effective area, and the positive pressure environment within the seed guide tube. It is jointly determined by the initial velocity of the seed-metering disc, the dynamic aerodynamic area related to the seed's posture, and the steady-state positive pressure of the seed guide tube. This provides a theoretical basis for optimizing the structure of the seed guide tube and the operational parameters.

5 Performance experiment

5.1 Experimental setup

To verify the operational performance of the pneumatic peanut seed dispensing device, this study constructed a pneumatic seeding comprehensive test platform based on the test method for single-seed (precision) seeders outlined in GB/T 6973-2005 (Figure 11). The test system comprises a pneumatic peanut seed-metering device, a motor-driven control device, a transparent steel wire pneumatic tube, a seed-metering device performance testing platform, a pressure measurement device, and an HG220 high-pressure vortex blower.

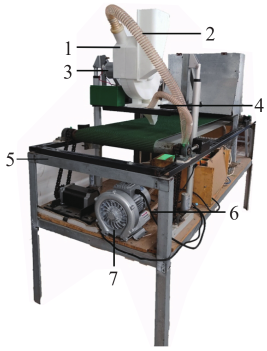

1. Pneumatic peanut precision seeder 2. Transparent steel wire pneumatic tube 3. Drive control device 4. Positive pressure seed-guiding device 5. Seed-metering device performance testing platform 6. Pressure measurement device 7. HG220 high-pressure vortex blower

Figure 11 Test bench

5.2 Experimental design and regression analysis

In this study, the evaluation indices were classified into two categories. Seed-metering performance was assessed by the qualified seed-metering rate, miss-seeding rate, and multiple-seeding rate, while seed-spacing performance was evaluated by the qualified seed-spacing rate in bench tests and by seed spacing uniformity rate and coefficient of variation in field tests. To avoid ambiguity, these terms were used consistently throughout the manuscript.

To investigate the effects of operating parameters on seed-metering performance, negative pressure (X_1), positive pressure (X_2), and seed-metering disc rotational speed (X_3) were selected as the experimental factors, while the qualified seed-metering rate (Y_1), miss-seeding rate (Y_2), multiple-seeding rate (Y_3), and qualified seed-spacing rate (Y_4) were used as evaluation indices. Based on the factor-level combinations listed in Table 3, a three-factor experimental design was carried out, and the test results are listed in Table 4. The experimental data were subsequently analyzed using Design-Expert 13.0.6 to establish quadratic regression models.

Table 3 Experimental factors and levels

Factor	Level 1	Level 2	Level 3
X_1 Negative pressure/kPa	5	6	7
X_2 Positive pressure/kPa	1	2	3
X_3 Rotational speed/r·min^{-1}	30	40	50

The factor combinations in Table 4 were used to fit the quadratic regression models for subsequent response analysis and multi-objective optimization.

The experimental data were imported into Design-Expert

13.0.6 software for regression analysis. Using the four performance indices as response variables and the three operating parameters as coded independent variables, quadratic polynomial regression models were constructed.The regression equations are as follows:

Qualified seed-metering rate (Y_1):

$$Y_1 = 90.88 + 0.7348A - 0.5506B - 6.40C + 0.6874AB - 0.6824AC - 0.9876BC - 6.82A^2 - 2.50B^2 - 1.22C^2$$

Miss-seeding rate (Y_2):

$$Y_2 = 6.64 - 0.6736A + 0.5418B + 5.63C - 0.7279AB + 0.6570AC + 0.8488BC + 6.17A^2 + 2.14B^2 + 1.09C^2$$

Multiple-seeding rate (Y_3):

$$Y_3 = 2.56 - 0.0634A + 0.0112B + 0.8336C + 0.2812AB + 0.0346AC + 0.1295BC + 0.8132A^2 + 0.5272B^2 - 0.1464C^2$$

Qualified seed-spacing rate (Y_4):

$$Y_4 = 95.56 + 1.61A - 2.32B - 1.65C - 0.1670AB - 0.6146AC + 0.6713BC - 4.25A^2 - 10.49B^2 - 0.3126C^2$$

Table 4 Experimental design scheme and results

Serial number	Experimental factors			Experimental indicators			
	X_1/kPa	X_2/kPa	X_3/r·min^{-1}	Y_1/%	Y_2/%	Y_3/%	Y_4/%
1	5	1	30	86.15	10.53	3.32	83.67
2	5	2	40	83.72	12.85	3.43	90.56
3	5	3	50	72.84	22.91	4.25	77.98
4	5	1	40	81.36	15.27	4.37	80.28
5	5	2	50	74.92	20.88	4.20	86.92
6	5	3	30	85.08	12.23	2.69	76.28
7	6	1	50	84.56	12.06	3.38	86.07
8	6	2	30	97.35	1.52	1.13	97.18
9	6	3	40	86.73	10.02	3.25	83.35
10	6	1	30	91.82	5.75	2.43	88.92
11	6	2	40	90.27	7.02	2.71	95.48
12	6	3	50	78.64	17.26	4.10	79.83
13	7	1	40	82.73	13.85	3.42	84.21
14	7	2	50	76.48	19.44	4.08	90.47
15	7	3	30	88.32	8.57	3.11	81.08
16	7	1	50	73.41	22.33	4.26	81.73
17	7	2	30	91.05	6.52	2.43	95.12
18	7	3	40	83.86	13.33	3.81	80.37

Regression analysis was conducted with Design-Expert 13.0.6, and quadratic polynomial models were obtained for all four performance indices.The analysis of variance (ANOVA) was conducted and the results are listed in Table 5. The analysis results showed that all four models passed the significance test (p<0.0001), indicating that the regression models were statistically significant and suitable for subsequent response analysis and parameter optimization.

To simplify the models and focus on the key factors that truly affect the evaluation indices, the significance of regression terms was screened through ANOVA (terms with p>0.05 were deemed insignificant). After eliminating redundant terms that had no substantial effect on the results, the following more concise significant regression models were finally obtained:

$$Y_1 = 90.88 - 6.40C - 6.82A^2 - 2.50B^2$$

$$Y_2 = 6.64 + 5.63C + 6.17A^2 + 2.14B^2$$

$$Y_3 = 2.56 + 0.8336C + 0.2812AB + 0.8132A^2 + 0.5272B^2$$

$$Y_4 = 95.56 + 1.61A - 2.32B - 1.65C - 4.25A^2 - 10.49B^2$$

Table 5 Analysis of variance for regression equations

Response variable	Source	Sum of squares	Degrees of freedom	Mean square	F	p
Qualification rate	Model	752.88	9	83.65	32.77	<0.0001
	A	5.83	1	5.83	2.28	0.1691
	B	3.27	1	3.27	1.28	0.2902
	C	443.03	1	443.03	173.56	<0.0001
	AB	3.19	1	3.19	1.25	0.2961
	AC	3.14	1	3.14	1.23	0.2994
	BC	6.58	1	6.58	2.58	0.1470
	A^2	179.15	1	179.15	70.18	<0.0001
	B^2	24.16	1	24.16	9.46	0.0152
	C^2	5.75	1	5.75	2.25	0.1716
	Residual	20.42	8	2.55	-	-
	Cor total	773.30	17	-	-	-
Miss-seeding rate	Model	596.61	9	66.29	36.82	<0.0001
	A	4.90	1	4.90	2.72	0.1376
	B	3.17	1	3.17	1.76	0.2212
	C	342.49	1	342.49	190.22	<0.0001
	AB	3.58	1	3.58	1.99	0.1964
	AC	2.91	1	2.91	1.62	0.2390
	BC	4.86	1	4.86	2.70	0.1389
	A^2	146.66	1	146.66	81.46	<0.0001
	B^2	17.66	1	17.66	9.81	0.0140
	C^2	4.62	1	4.62	2.57	0.1478
	Residual	14.40	8	1.80	-	-
	Cor total	611.01	17	-	-	-
Re-sowing rate	Model	11.60	9	1.29	15.78	0.0003
	A	0.0435	1	0.0435	0.5322	0.4865
	B	0.0013	1	0.0013	0.0165	0.9011
	C	7.51	1	7.51	91.87	<0.0001
	AB	0.5338	1	0.5338	6.53	0.0339
	AC	0.0081	1	0.0081	0.0991	0.7610
	BC	0.1133	1	0.1133	1.39	0.2729
	A^2	2.55	1	2.55	31.22	0.0005
	B^2	1.07	1	1.07	13.12	0.0068
	C^2	0.0826	1	0.0826	1.01	0.3440
	Residual	0.6536	8	0.0817	-	-
	Cor total	12.25	17	-	-	-
Seed-spacing qualification rate	Model	649.67	9	72.19	41.60	<0.0001
	A	27.95	1	27.95	16.11	0.0039
	B	58.10	1	58.10	33.49	0.0004
	C	29.26	1	29.26	16.86	0.0034
	AB	0.1883	1	0.1883	0.1085	0.7503
	AC	2.55	1	2.55	1.47	0.2600
	BC	3.04	1	3.04	1.75	0.2221
	A^2	69.60	1	69.60	40.12	0.0002
	B^2	424.21	1	424.21	244.50	<0.0001
	C^2	0.3769	1	0.3769	0.2172	0.6536
	Residual	13.88	8	1.74	-	-

5.3 Analysis of factor effects

Based on the regression equations of the four evaluation indices, the relative significance of the influencing factors was determined. For the qualified seed-metering rate (Y_1), the factors were ranked in the order of seed-metering disc rotational speed (C)

and fan negative pressure (A). For the miss-seeding rate (Y_2), the primary and secondary influencing factors were also seed-metering disc rotational speed (C) and fan negative pressure (A). For the multiple-seeding rate (Y_3), the order of factor significance remained seed-metering disc rotational speed (C) followed by fan negative pressure (A). In contrast, for the qualified seed-spacing rate (Y_4), the influencing factors were ranked in the order of positive pressure of the seed-guiding device (B), fan negative pressure (A), and seed-metering disc rotational speed (C). The response surface plots of the evaluation indices are shown in Figure 12.

5.4 Parameter optimization and verification

Through multi-objective optimization, the optimal parameter combination was determined as follows: negative pressure of 6.08 kPa, positive pressure of 2.05 kPa, and rotational speed of 32 r/min. Under this parameter combination, the predicted values were a qualified seed-metering rate of 96.28%, a miss-seeding rate of 2.15%, a multiple-seeding rate of 1.57%, and a qualified seed-spacing rate of 97.61%. The relative error between the predicted and measured values was less than 1%, indicating that the regression models had good predictive accuracy. The results also showed that negative pressure was the key regulating factor and needed to be coordinated with positive pressure and rotational speed to achieve improved seed-metering performance. The optimized negative pressure of 6.08 kPa obtained from regression analysis is close to the optimal discrete level of 6.0 kPa identified by the Fluent-EDEM coupled simulation, indicating good consistency between the two optimization approaches.

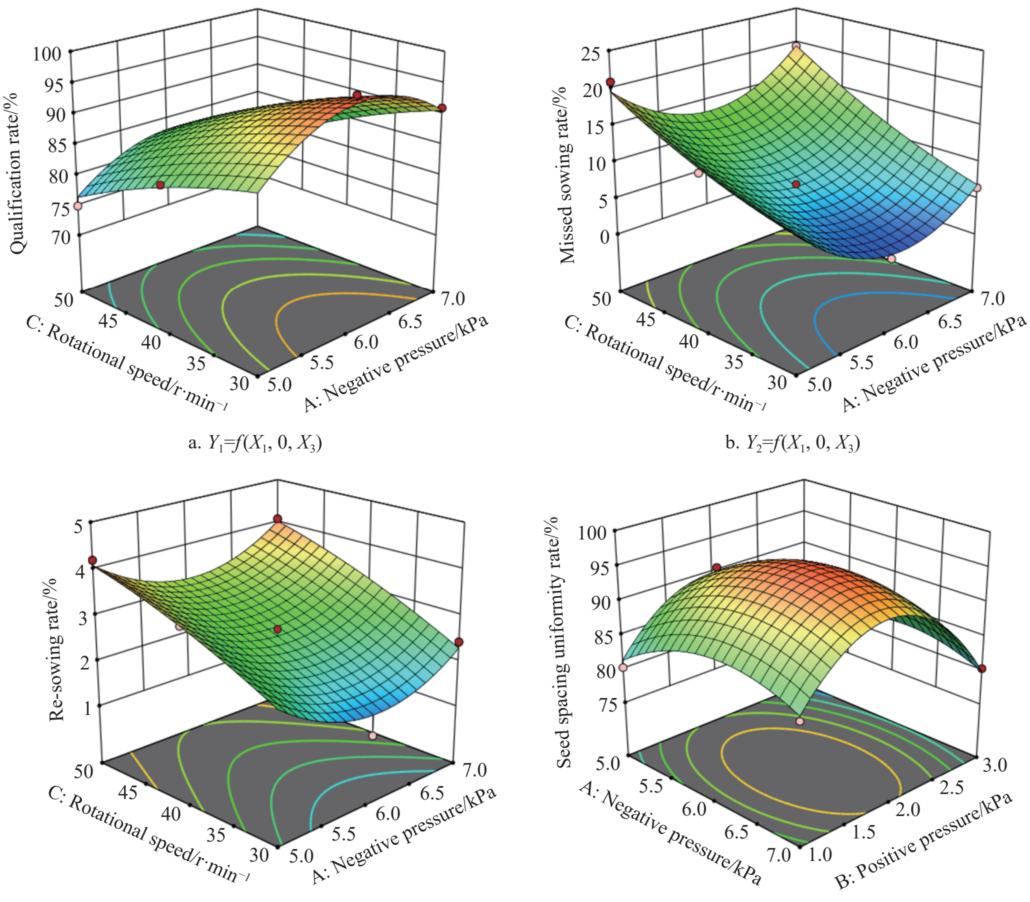

a. $Y_1=f(X_1, 0, X_3)$ b. $Y_2=f(X_1, 0, X_3)$

c. $Y_3=f(X_1, 0, X_3)$ d. $Y_4=f(X_1, 0, X_3)$

Figure 12 Response surface plots of the evaluation indices

Figure 13 Field performance test diagram

5.5 Field experiment

After the performance of the seed-metering device was verified to meet the requirements through bench tests, a field experiment on seeding performance was conducted in Zhuqiao Town, Laizhou City, Yantai City, Shandong Province to test its actual working effect. A Lovol M2404 tractor was used for traction operation, with a seeding pattern of three ridges and six rows (Figure 13). The left seed-metering device of the seeder was removed, and the seed-metering device developed in this study was installed and adapted.

The cultivated area for the experiment was 500 m^2, with a working width of 3.5 m, adopting a three-ridge and six-row pattern (2 rows per ridge) and a row spacing of 25 cm.

Based on the bench optimization results, the negative pressure of the seed-metering device was set to 6.0 kPa and the positive pressure of the seed-guiding device was set to 2.0 kPa during the field tests. Field experiments were conducted at operating speeds of 6, 8, 10, 12, and 14 km/h. For each operating speed, three replications were performed, and data were collected only from the stable operating section to eliminate the influence of machine acceleration and deceleration. In each replicate, seed-spacing data were measured continuously over a fixed test length, and the mean values were used for analysis. The field performance indices included seed spacing uniformity rate, miss-seeding rate, multiple-seeding rate, and coefficient of variation of seed spacing.

After analyzing the field test results in Table 6, the influence of different operating speeds (6-14 km/h) on seed metering performance was explored. At 6 km/h, the qualified seed-metering rate reached 93.35%, while the miss-seeding rate, multiple-seeding rate, and coefficient of variation remained low, indicating good sowing quality. From 8 km/h onwards, the seed metering stability gradually decreased but still met general requirements. At 10 km/h, the seeding quality declined, but it had certain practicality in efficiency-prioritized scenarios. At 12 km/h, due to the poor adaptation between the seed metering mechanism and the airflow field, miss-seeding and multiple-seeding increased, resulting in below-average quality. When the field operating speed was ≤ 12 km/h, the performance indices of the seed-metering device met the national standards for precision seeding.

Table 6 Results of field experiment

Speed/ $km \cdot h^{-1}$	Qualified seed-metering rate/%	Miss-seeding rate/%	Multiple-seeding rate/%	Qualified seed-spacing rate/%
6	93.35	3.86	2.79	3.25
8	92.13	4.68	3.19	3.95
10	89.73	5.85	4.42	5.33
12	84.95	8.31	6.74	7.86
14	76.83	14.45	8.72	11.33

Field test data show that the seed-metering device performed stably at operating speeds from 6 to 12 km/h, with the qualified seed-spacing rate above 84.95% and the miss-seeding rate below 8.31% in this range. A noticeable decline in sowing quality occurred at 14 km/h, suggesting the device is more suitable for medium-to-high speed operations within 12 km/h.

6 Conclusions

1) Based on the measured geometric characteristics of "Silihong" peanut seeds, with average length, width, and thickness of 14.3 mm, 7.8 mm, and 7.4 mm, respectively, a matched seed-metering disc with a diameter of 255 mm, 21 suction holes, and a suction-hole diameter of 6.2 mm was designed. DEM simulation results showed that the optimized spoke-wing groove disturbing structure with a groove depth of 4 mm and groove length of 40 mm increased the average seed-population velocity from 0.1373 m/s to 0.1706 m/s, indicating improved seed-population fluidization and seed-filling performance.

2) Fluent-EDEM gas-solid coupling simulation indicated that 6 kPa was the optimal negative pressure, at which the single-seed adsorption rate reached 98.6%, while miss-adsorption at 5 kPa and multiple adsorption at 7 kPa were effectively avoided. Based on the regression optimization of bench-test data, the optimal working parameter combination was determined as a negative pressure of 6.08 kPa, a positive pressure of 2.05 kPa, and a seed-metering disc rotational speed of 32 r/min, corresponding to a qualified seed-metering rate of 96.28%, a miss-seeding rate of 2.15%, a multiple-seeding rate of 1.57%, and a qualified seed-spacing rate of 97.61%.

3) Field tests showed that the developed seed-metering device maintained relatively stable performance at operating speeds of 6-12 km/h. Within this range, the qualified seed-metering rate remained above 84.95%, and the miss-seeding rate remained below 8.31%. When the operating speed increased to 14 km/h, sowing quality deteriorated noticeably, indicating that the current structure is more suitable for medium-speed and moderately high-speed operation.

However, this study has limitations: the seed-metering device was optimized specifically for "Silihong" peanuts, with adaptability to other varieties (e.g., differing in size) yet to be verified. Field trials were limited to Zhuqiao Town, Shandong, requiring further validation across diverse soils, climates, and agronomic practices for broader generalizability.

Acknowledgements

This work was supported by the Shandong Province Key Research and Development Program (Agricultural Seed Improvement Project) under Grant No. 2024LZGC004.

[References]

[1] Tiwari J K, Mishra Y K, Tiwari B, Singh A, Chandra Joshi D, Kumar A. Groundnut (*Arachis hypogaea*): The protein-rich oilseed of adaptability and nutrition. Kumar A, Tiwari J K, Chandra Joshi D, Varshney R K, eds. Fasting superfoods. Singapore: Springer Nature Singapore, 2026; pp.3–26. DOI: 10.1007/978-981-95-2762-5_1.

[2] Qiu Q S, Li Z C, Shen F Y. Nutritional value of peanuts. Peanut Science and Technology, 1998; 3: 15–19.

[3] Raza A, Abdullaziz S, Wang X, Zhang X, Varshney R K, Zhuang W. An introduction to peanut importance, genomics, and biotechnology: Past, present, and future outlooks. Peanut genomics and biotechnology, Boca Raton: CRC Press, 2026; pp.1–16. DOI: 10.1201/9781003360988-1.

[4] Wu J X, Wu Y, Sun Q Q, Sun K Z, Chi Y C, Wu Z F, et al. Effects of different cultivation techniques on agronomic traits and sensory quality of Japanese fresh-eating peanut Omasari. Chinese Journal of Oil Crop Sciences, 2023; 45(5): 916–922.

[5] Gelaye Y, Luo H. Optimizing peanut (*Arachis hypogaea* L.) production: Genetic insights, climate adaptation, and efficient management practices: Systematic review. Plants, 2024; 13(21): 2988.

[6] Asif M, Rayamajhi A, Mahmud M S. Technological progress toward peanut disease management: A review. Sensors, 2025; 25(4): 1255.

[7] Sun Y H, Guo J H, Shi L R. Design and parameter optimization of air-suction wheel type of seed-metering device with elastic pad for maize. Int J Agric & Biol Eng, 2024; 17(4): 116–127.

[8] Feng Y B, Zhao X S, Li J C, Yu H L, Zhao H P, Yin B Z. Parameter optimi zation and experiment of the negativepressure precision seed-metering device for wheat. Int J Agric & Biol Eng, 2024; 17(1): 154–162.

[9] Liao X, Xie H, Hu Z, Wang J, Liu M, An J, et al. Peanut-shelling technologies and equipment: A review of recent developments. Agriculture, 2024; 14(7): 1178.

[10] Xing H, Wang Y W, Chen Y B, Yang R, Bo X Z, Zang Y. Experiment and analysis of seed suction model for rice pneumatic seed metering device using DEM-CFD approach. Int J Agric & Biol Eng, 2025; 18(5): 191–197.

[11] Zhao X S, Zhao H P, Wang Z H, Li J C, Yu H L, Yan Q. Electronic control seed-metering system for precision seeding maize based on fuzzy PID. Int J Agric & Biol Eng, 2024; 17(4): 217–226.

[12] Shah K, Alam M S, Nasir F E, Qadir M U, Ul Haq I, Khan M T. Design and performance evaluation of a novel variable rate multi-crop seed metering unit for precision agriculture. IEEE Access, 2022; 10: 133152–133163.

[13] Yu Y, Tan X Z, Li G Y, Yi D Z, Wang X M, Dong W K. Design and experiment of an online monitoring system for peanut seeding parameters

based on IoT. Int J Agric & Biol Eng, 2025; 18(3): 186–194.
[14] Monosem. MECA V4E metering unit. Available at: http://www.monosem.com/News/Products-and-news/MECA-V4E-Metering-unit. Accessed on: 2024-12-25.
[15] Dahlstrom N. Tractor wars: John Deere, Henry Ford, International harvester, and the birth of modern agriculture. Dallas: BenBella Books, 2022.
[16] He D J, Li Z W. Study on seed movement and parameters of air-suction seed metering device with combined suction holes. Journal of Northwest A& F University (Natural Science Edition), 1995; 6: 33–37.
[17] Chen J, Li Y M, Wang X Q, Zhao Z. Finite element analysis of airflow field in suction holes of air-suction seed metering device. Transactions of the CSAM, 2007; 38(9): 59–62.
[18] Yi S J, Chen T, Li Y F, Tao G X, Mao X. Design and test of millet hill-drop seed-metering device with combination of positive-negative pressure and hole wheel. Transactions of the CSAM, 2021; 52(6): 83–94.
[19] Tang H, Xu F, Guan T, Xu C, Wang J. Design and test of a pneumatic type of high-speed maize precision seed metering device. Computers and Electronics in Agriculture, 2023; 211: 107997.
[20] Zhang M H, Jiang Y C, He S Y, Huang Z S, Qin W, Qian C, et al. Design and experiment of the air suction wheel precision seed metering device for vegetables. Transactions of the CSAE, 2023; 39(7): 98–109. (in Chinese)
[21] Guan X, Nie S, Ge H, Ding Y, Yang J. Research status and development trends of adjustable precision seeders. Agronomy, 2026; 16(5): 495.
[22] Lu J, Liu S, Wang Q, Liao M. Research on device and sensing technology for precision seeding of potato. Agriculture, 2024; 14(12): 2146.
[23] Liu H, Liao Y T, Wang L, Wang B S, Du Z, Liao Q X. Design and experiment of positive and negative pressure combination precision metering device for pakchoi. Transactions of the CSAM, 2022; 53(10): 54–65. (in Chinese)
[24] Zhao L Q, Chen M X, Xu S, Meng Y X, Liu B H. Design and test on the seed metering device of suction-type *Cyperus esculentus* precision planter. Journal of Jilin Agricultural University, 2022; 4: 1–9. (in Chinese)
[25] Wang F Y, Yang L, Bao Y F, Jiang J T. Development of air-suction ridging and seeding machine for carrot. Transactions of the CSAE, 2020; 36(17): 35–45. (in Chinese)
[26] Dong J, Wu J, Zhu Y, Gao X. Investigation on seed-filling effect of quantitative precision filling high-speed seed-metering device for maize. Agriculture, 2025; 15(14): 1517.
[27] Zhuang Y, Han J, Liu Z, Zhang M, Zhang Z, Lan Y, et al. Optimum design of seed holding ring of vertical disc seed-metering device. INMATEH-Agricultural Engineering, 2022; 66(1): 219–228.
[28] Tempelmeyer I J. Flex-Ro: Development and testing of a semi-autonomous robotic planter. Lincoln, NE: University of Nebraska-Lincoln, 2023.
[29] Sun Q T, Sun W X, Liu L, Liu D Q, Qian K, Chen K Y, et al. Trial production of two-row ridge-cultivated peanut digging, turning, drying and harvesting machine. Journal of Peanut Science, 2025; 54(1): 87–95.
[30] Wang G W, Xia X M, Zhu Q H, Yu H Y, Huang D Y. Design and experiment of soybean high-speed precision vacuum seed metering with auxiliary filling structure based on DEM-CFD. Journal of Jilin University (Engineering and Technology Edition), 2022; 52(5): 1208–1221.
[31] Guo J, Yang Y, Memon M S, Tan C, Wang L, Tang P, et al. Design and simulation for seeding performance of high-speed inclined corn metering device based on discrete element method (DEM). Scientific Reports, 2022; 12(1): 19415.
[32] Huang P, Pan X, Niu Y, Du L. Concrete failure simulation method based on discrete element method. Engineering Failure Analysis, 2022; 139: 106505.
[33] Liu R, Liu Z, Zhao J, Lu Q, Liu L, Li Y. Optimization and experiment of a disturbance-assisted seed filling high-speed vacuum seed-metering device based on DEM-CFD. Agriculture, 2022; 12(9): 1304.
[34] Xie D B, Zhang C L, Wu X Q, Wang W W, Liu L C, Chen L Q. Design and test of garlic seed placer with seed disturbing tooth assisted air suction. Transactions of the CSAM, 2022; 53(2): 47–57. (in Chinese)
[35] Lü Y C. Design and experiment of wheat seed metering device with disturbing seed and trapezoidal hole wheel. Zibo: Shandong University of Technology, 2023.
[36] Wang D W, Ji R Q, He X N, Guo P, Shi Y X, Zhang C X. Study on air-suction high-speed precision peanut seed metering device with driving-guide combined groove assisted seed attachment. Transactions of the CSAM, 2023; 54(5): 59–70, 149. (in Chinese)